Electronic Supplementary Material (ESI) for Journal of Materials Chemistry C.

Electric field recoverable large shape memory in BNT-based lead-free ceramics

He Qi,[abc] Liang Chen,[ab] Huajie Luo,[ab] Hui Liu,[ac] Shiqing Deng,[ac] Xianran Xing,[ab] and Jun Chen*[abc]

[a]Beijing Advanced Innovation Center for Materials Genome Engineering, University of Science and Technology Beijing, Beijing 100083, China.

[b]Department of Physical Chemistry, University of Science and Technology Beijing, Beijing 100083, China

[c]School of Mathematics and Physics, University of Science and Technology Beijing, Beijing 100083, China.

*Corresponding author: junchen@ustb.edu.cn

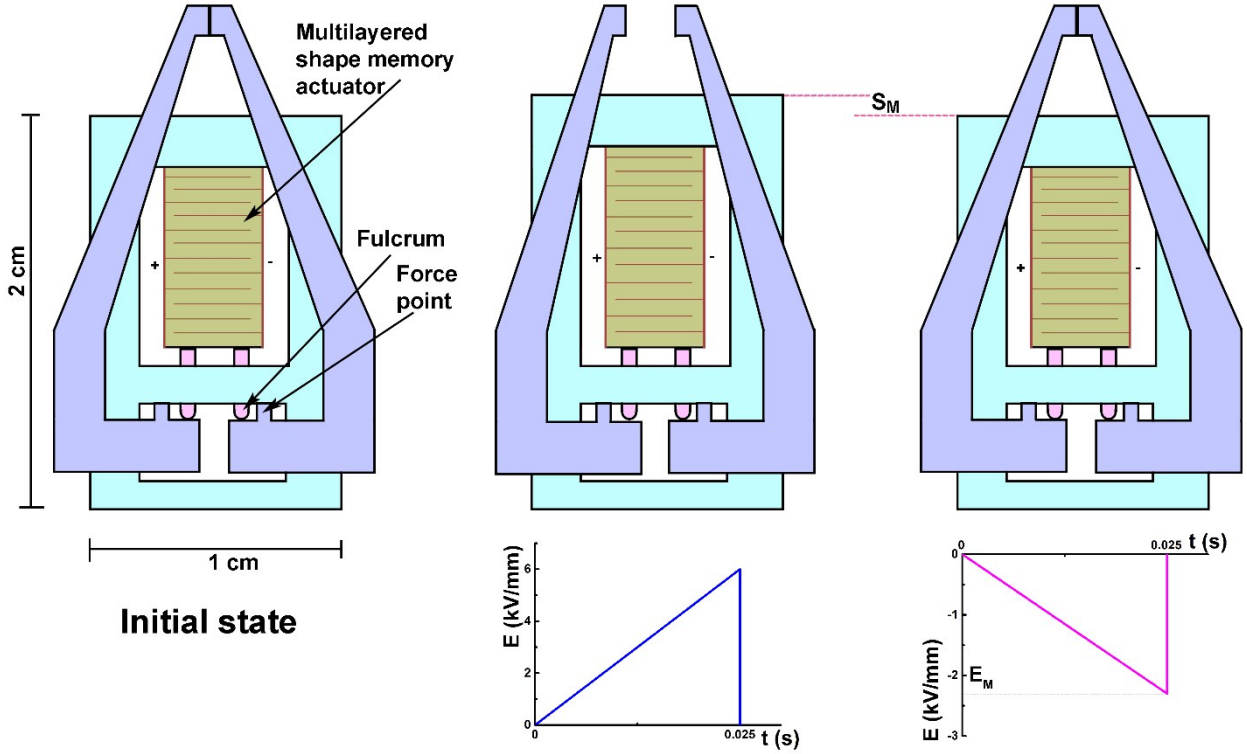

Fig. S1 Construction and the working principle of the mechanical clamper using a shape memory actuator. The state of "open" and "close" can be maintained without holding electric field.

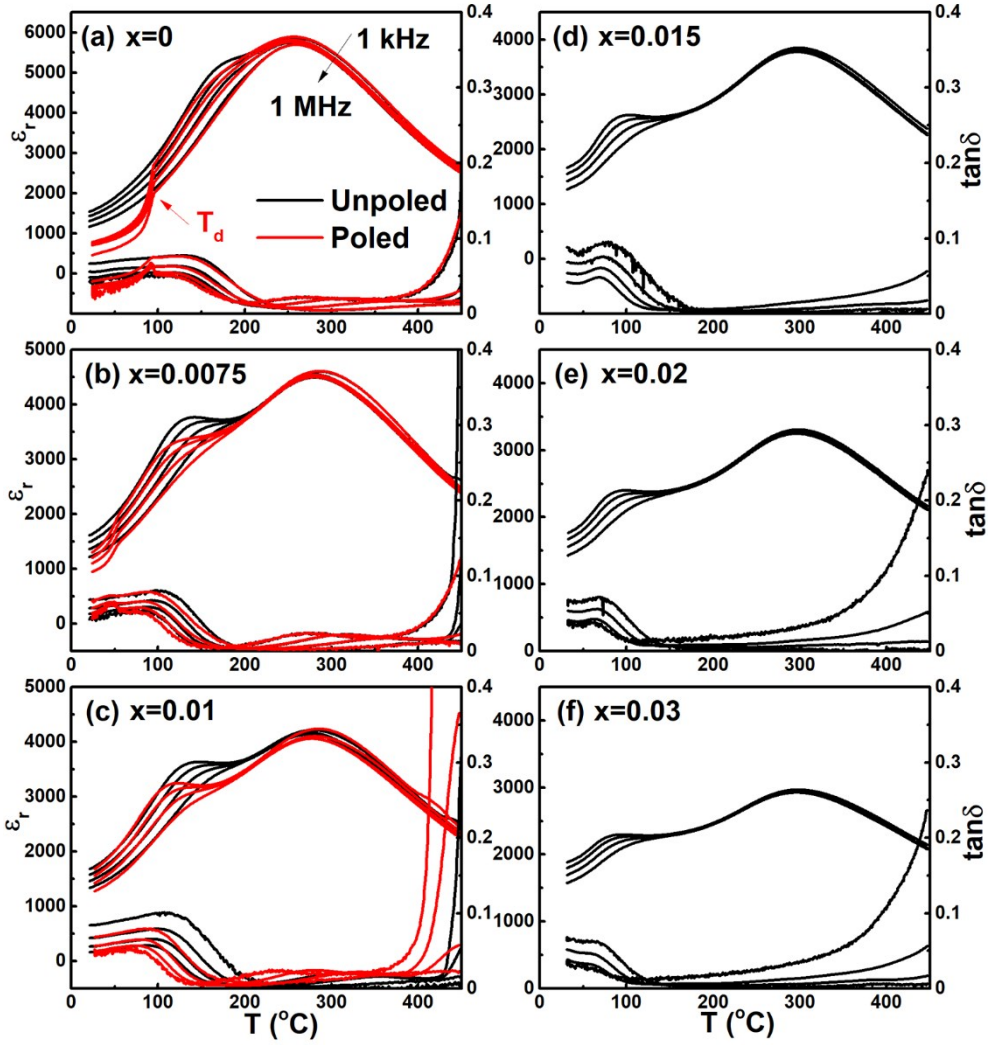

Fig. S2 Temperature and frequency dependent dielectric permittivity and loss tangent for unpoled and poled BNBT-*x*Ta ceramics: (a) *x*=0, (b) *x*=0.0075, (c) *x*=0.01, (d) *x*=0.015, (e) *x*=0.02 and (f) *x*=0.03.

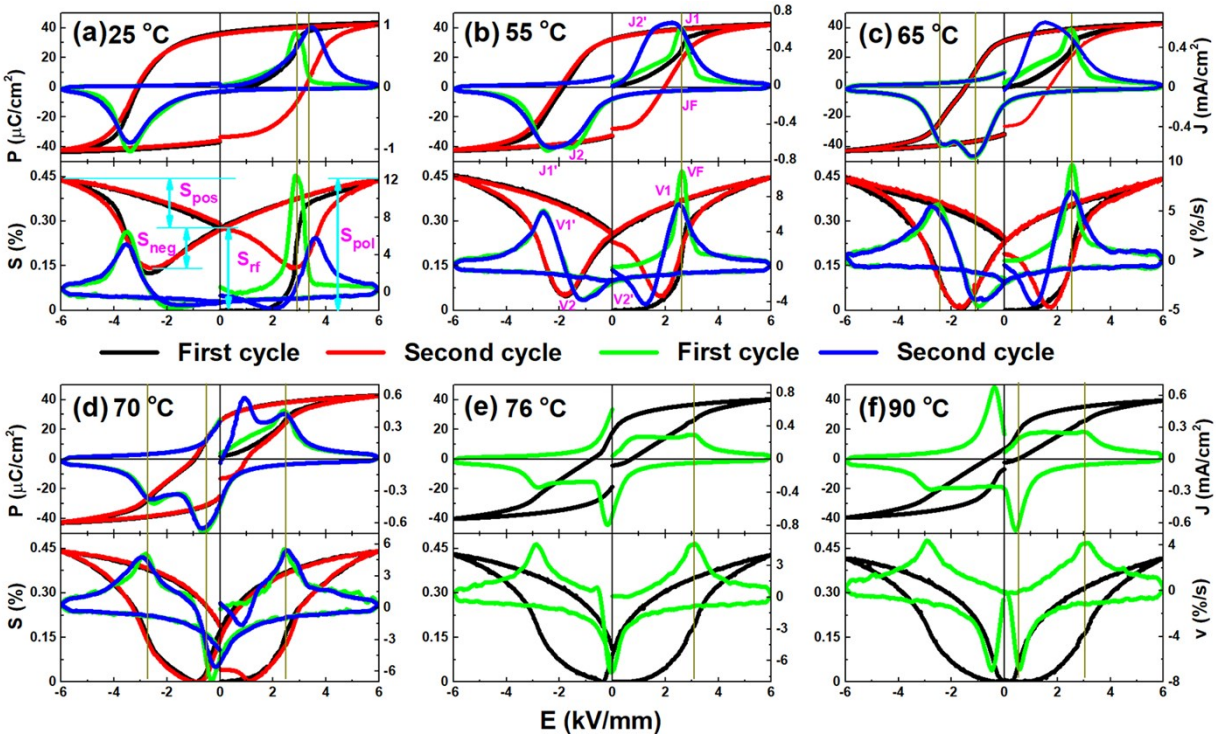

Fig. S3 Temperature dependent *P*-*E*, *J*-*E*, *S*-*E* and *v*(=*dS*/*dE*)-*E* loops for the BNBT-0Ta ceramic measured at different electric field cycles.

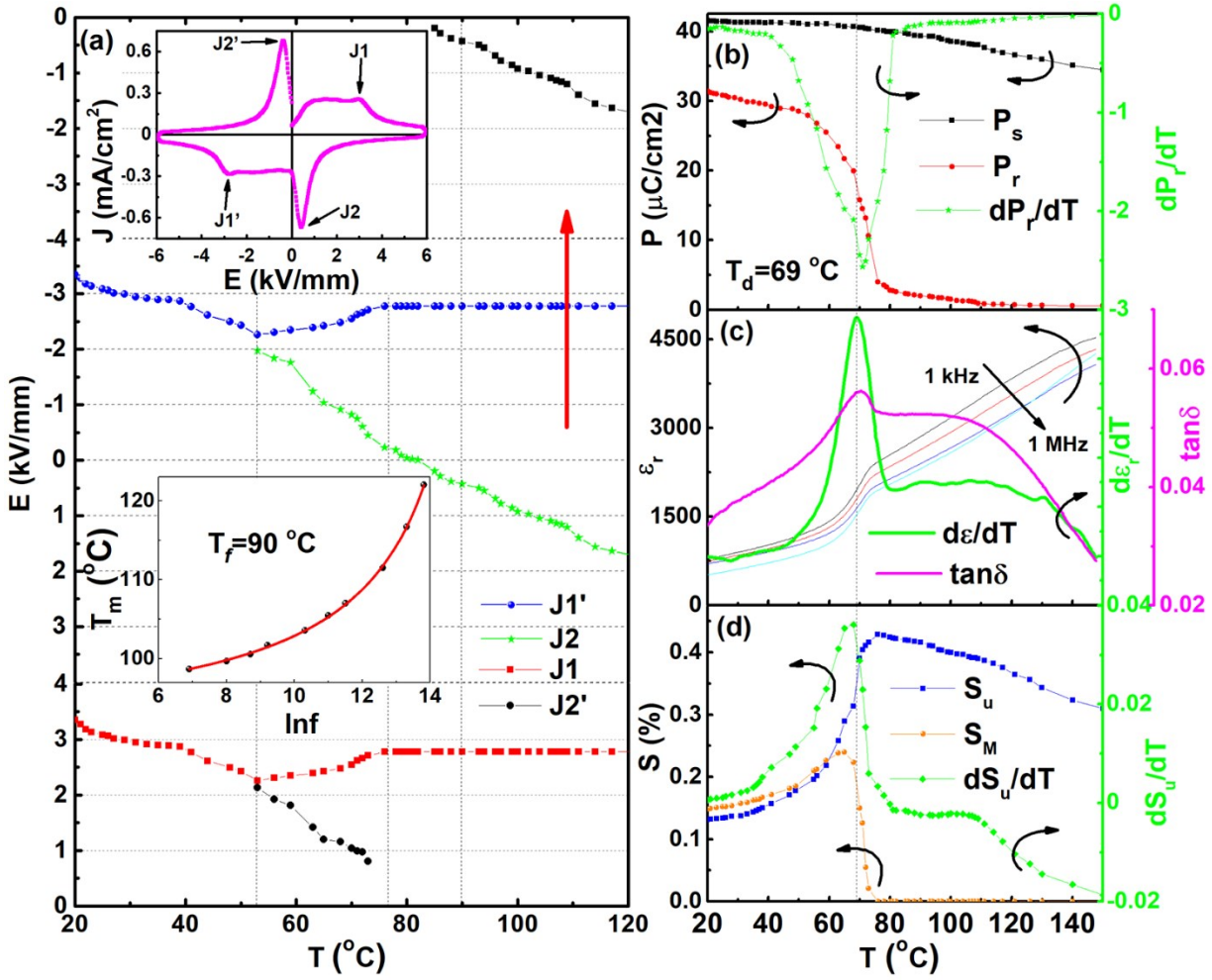

Fig. S4 (a) Temperature-electric field phase diagram of BNBT-0Ta ceramic. The evolution of (b) P_s, P_r, dP_r/dT, (c) ε_r, $d\varepsilon_r/dT$, $tan\delta$, (d) S_u, S_M and dS_u/dT with changing temperature.

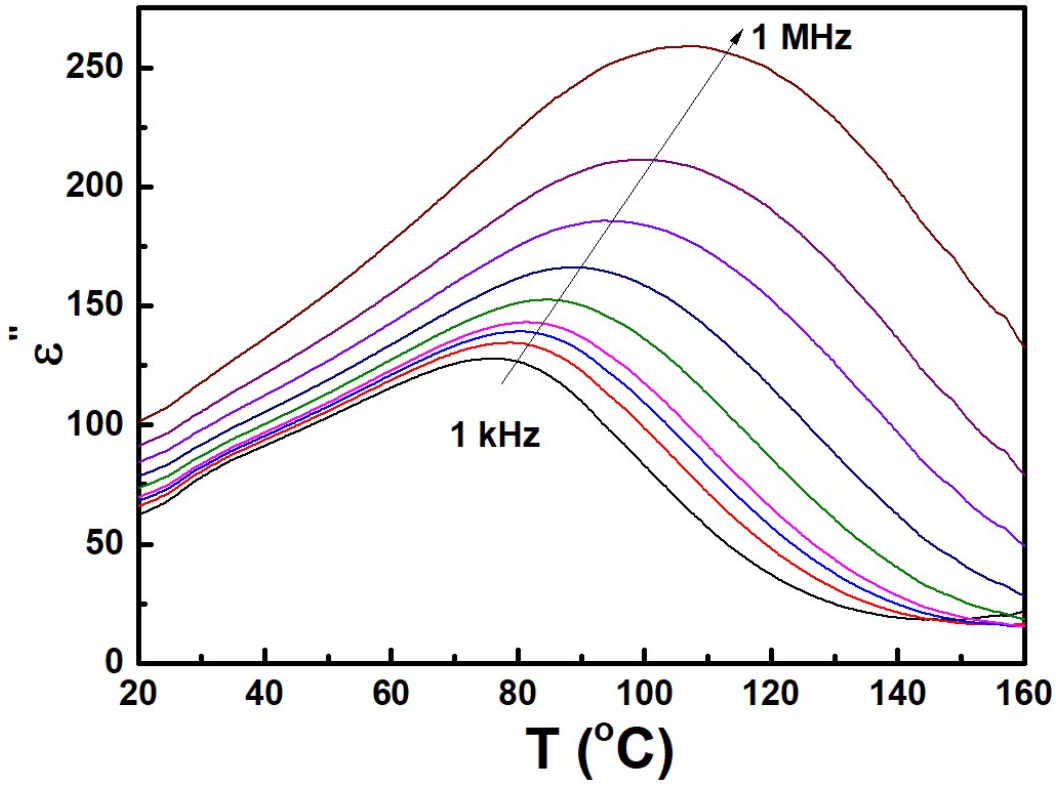

Fig. S5 The imaginary part of the dielectric permittivity ε'' as a function of temperature at various frequencies for the x=0.0075 ceramic measured during cooling. The temperature of the maximum ε'' was taken as T_m for *V-F* law fitting.

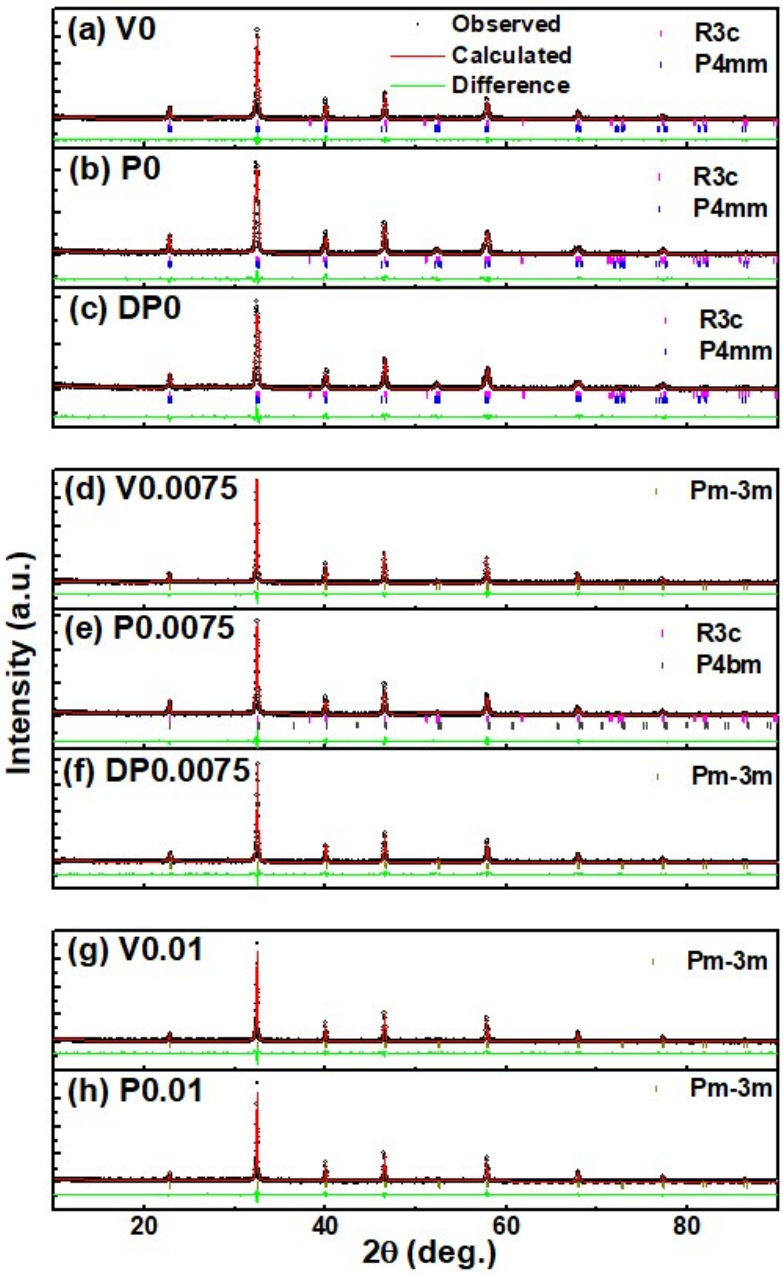

Fig. S6 Rietveld refinement results on the conventional XRD patterns of BNBT-*x*Ta ceramic powders after treatment under different electric field conditions. V: virgin, P: poled under 6 kV/mm, DP: poled under 6 kV/mm and then depolarized the d_{33} to zero by a reverse electric field. The data was obtained by a powder x-ray diffractometer (D/Mzx-rB; Rigaku, Tokyo, Japan) with Cu Kα radiation under an acceleration condition of 40 kV and 30 mA. Different from the high energy SXRD, a pseudocubic Pmm phase was used for the virgin *x*=0.0075 sample owing to the relatively low resolution of conventional XRD.

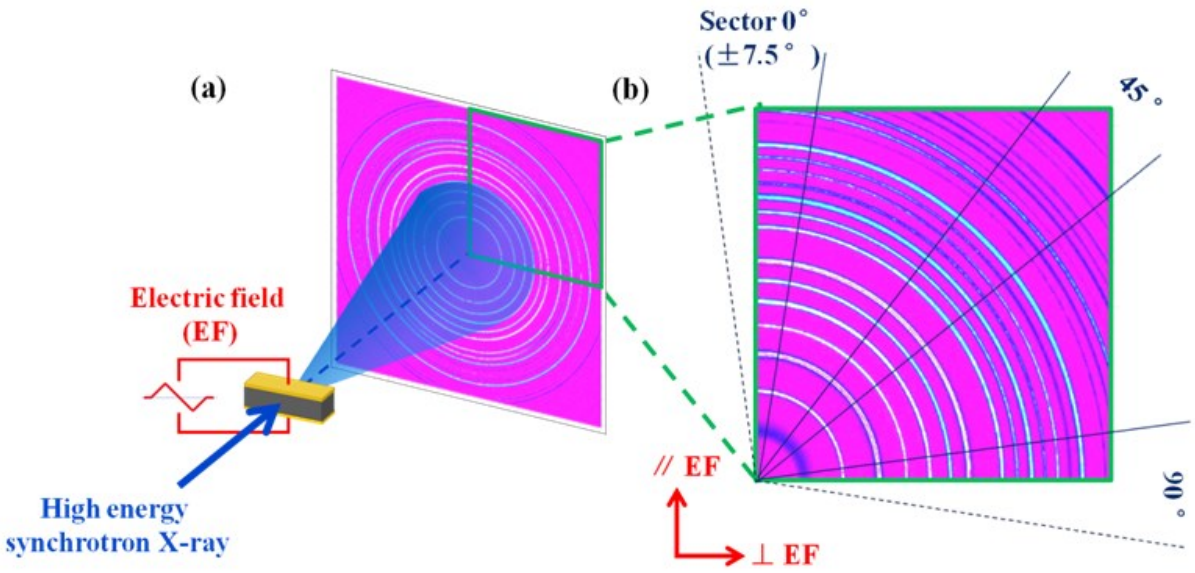

Fig. S7 Schematic of the experimental setup for in-situ high-energy synchrotron X-ray diffraction experiments.

For the in-situ high-energy SXRD measurements, the ceramic samples were polished, cut into rectangular bars with dimensions of 6 mm×1 mm×0.6 mm, and then annealed at 500 °C for 6 h to release stresses. Gold electrodes with a size of 6 mm×1 mm were evaporated on opposite faces of the bars. The in-situ high-energy SXRD measurements were conducted at the 11-ID-C beamline at the Advanced Photon Source (APS) at the Argonne National Laboratory. The X-ray beam with a spot size of 0.5 mm×0.5 mm, photon energy of about 110 keV and a wavelength of 0.11165 Å were used. A Perkin Elmer amorphous silicon 2D detector, positioned approximately 1800 mm away from the sample, was used to collect the scattered photons. The direction of the electric field was perpendicular to the X-ray beam. A triangular bipolar cycle electric field (−6 kV/mm ~ +6 kV/mm) with a step of about 0.4 kV/mm was applied to the ceramic samples. At each step, a diffraction pattern was recorded with an acquisition time of 30 s, which is equivalent to a cyclic frequency around 40 mHz. The diffraction pattern of Ceria standard was used to

calibrate the detector related parameters. The Debye rings collected on the 2D detector were divided into equidistant sectors at 15°. Intensities of the X-ray diffraction peaks in the sectors were integrated using the Fit2d software.

Table S1. Refined structural parameters achieved from Fig. S4 for BNBT-*x*Ta ceramics measured at room temperature.

x	State	Space group	Lattice parameters	V (Å^3)	R_{wp} (%)	R_p (%)	χ^2
0	Virgin	R3c 71% P4mm 29%	a=b=5.5061(2) Å, c=13.5839(5) Å, α=β=90°, γ=120° a=b=3.8921(2) Å, c=3.9363(2) Å, α=β=γ=90°	356.221(18) 59.629(3)	9.69	7.97	1.34
0	Poled	R3c 37% P4mm 63%	a=b=5.5052(1) Å, c=13.5902(4) Å, α=β=90°, γ=120° a=b=3.8943(1) Å, c=3.9391(2) Å, α=β=γ=90°	356.708(12) 59.740(3)	9.92	7.47	1.24
0	Depoled	R3c 40% P4mm 60%	a=b=5.5051(2) Å, c=13.5818(6) Å, α=β=90°, γ=120° a=b=3.8957(1) Å, c=3.9349(3) Å, α=β=γ=90°	356.470(13) 59.720(3)	9.24	7.60	1.21
0.0075	Virgin	Pmm	a=b=c=3.9024(1) Å, α=β=γ=90°	59.429(2)	9.67	7.93	1.30
0.0075	Poled	R3c 82% P4bm 18%	a=b=5.5146(2) Å, c=13.5441(4) Å, α=β=90°, γ=120° a=b=5.5087(2) Å, c=3.9202(1) Å, α=β=γ=90°	356.714(16) 118.964(4)	9.21	7.68	1.30
0.0075	Depoled	Pmm	a=b=c=3.9034(1) Å, α=β=γ=90°	59.476(3)	9.50	7.75	1.38
0.01	Virgin	Pmm	a=b=c=3.9023(1) Å, α=β=γ=90°	59.427(3)	9.85	8.19	1.40
0.01	Poled	Pmm	a=b=c=3.9022(1) Å, α=β=γ=90°	59.420(3)	9.76	8.20	1.38